Reports of Practical Oncology and Radiotherapy 25 (2020) 233–240

Available online at www.sciencedirect.com

Reports of Practical Oncology and Radiotherapy

journal homepage: http://www.elsevier.com/locate/rpor

Original research article

# Application of the phase-space distribution approach of Monte Carlo for radiation contamination dose estimation from the (n,γ), (γ,n) nuclear reactions and linac leakage photons in the megavoltage radiotherapy facility

Amir Ghasemi-Jangjoo[a,b], Hosein Ghiasi[a,*]

[a] Medical Radiation Sciences Research Team, Imam Hospital, Tabriz University of Medical Sciences, Imam Hospital, Tabriz, Iran
[b] Department of Radiology and Radiotherapy, Medicine School, Tabriz University of Medical Sciences, Imam Hospital, Tabriz, Iran

ARTICLE INFO

*Article history:*
Received 12 July 2019
Received in revised form
24 December 2019
Accepted 20 January 2020
Available online 24 January 2020

*Keywords:*
Phase-space distribution
Monte Carlo simulation
Dose equivalent
Photon
Neutron

ABSTRACT

*Aim:* The aim of this study was to characterize the radiation contamination inside and outside the megavoltage radiotherapy room.
*Background:* Radiation contamination components in the 18 MV linac room are the secondary neutron, prompt gamma ray, electron and linac leakage radiation.
*Materials and Methods:* An 18 MV linac modeled in a typical bunker employing the MCNPX code of Monte Carlo. For fast calculation, phase-space distribution (PSD) file modeling was applied and the calculations were conducted for the radiation contamination components dose and spectra at 6 locations inside and outside the bunker.
*Results:* The results showed that the difference of measured and calculated percent depth-dose (PDD) and photo beam-profile (PBP) datasets were lower than acceptable values. At isocenter, the obtained photon dose and neutron fluence were $2.4 \times 10^{-14}$ Gy/initial e° and $2.22 \times 10^{-8}$ n°/cm$^2$, respectively. Then, neutron apparent source strength ($Q_N$) value was found as $1.34 \times 10^{12}$ n°/Gy X at isocenter and the model verified to photon and neutron calculations. A surface at 2 cm below the flattening filter was modeled as phase-space (PS) file for PDD and PBP calculations. Then by use of a spherical cell in the center of the linac target as a PS surface, contaminant radiations dose, fluence and spectra were estimated at 6 locations in a considerably short time, using the registered history of all particles and photons in the 13GB PSD file as primary source in the second step.
*Conclusion:* Designing the PSD file in MC modeling helps user to solve the problems with complex geometry and physics precisely in a shorter run-time.
© 2020 Greater Poland Cancer Centre. Published by Elsevier B.V. All rights reserved.

## 1. Background

The shielding of radiological facilities against photon and neutron exposure is a requirement to prevent the radiation-induced malignancies in patients and staff in radiation therapy departments. Concrete is the primary material recommended for the design of a megavoltage bunker; in radiography departments, however, lead is the main shielding material. The characteristics of concrete and the improvement of shielding against radiation have been the subject of multiple studies.[1–6] Additionally, the capabilities of the Monte Carlo (MC) all-purpose N-Particle transport code (MCNP) and other computational methods to solve the complex problems of the radiological field have been revealed and application of the code to different radiological problems has been increasingly reported in the literature as well as neutron dosimetry in mixed field dosimetry.[7–10] International Commission on Radiation Units and measurement (ICRU) in report no. 26, which discussed neutron dosimetry for biology and medicine, reported that dosimetry in neutron-gamma mixed radiation field should be conducted by at least 2 dosimeters, one sensitive to gamma ray and the other to neutron. The dosimeter applied in this study conducted dosimetry in a gamma-neutron mixed radiation field.[8]

Moreover, MC simulation must be conducted by an experienced user, as this is a fact that employment of modeling approach for MC simulation, making it strong, powerful, and fast-operating method, compared with a full MC simulation. Modeling involves the application of knowledge to the problem and reduction of the

* Corresponding author.
*E-mail address:* hoseinghiasi62@gmail.com (H. Ghiasi).

https://doi.org/10.1016/j.rpor.2020.01.006
1507-1367/© 2020 Greater Poland Cancer Centre. Published by Elsevier B.V. All rights reserved.

dispensable complexity of an input file, which includes essential information and avoids unnecessary information. Modeling procedures improve the precision of the results in the shortest possible run time. For example, simple linac model simulations yield good results that can often provide sufficient information.[11–18]

One of the main aims of MC code users is to obtain the best results in as short a time as possible. MC simulation is applied within a range of radiological fields, including radiation therapy, dosimetry, and treatment planning, as well as radiation source characterization, nuclear medicine, and radiation distribution mapping. Importantly, using MC methods, dosimetric parameters related to a radiation therapy facility including linear accelerator (Linac) and its bunker can be scrutinized.[15–18] MC simulation of medical Linacs and characterization of electron and photon beams have been the subject of numerous studies in radiation physics.[19] Mesbahi et al. used the MCNP code to estimate photoneutron and capture gamma ray doses from a verified linac in different rooms and within multiple maze layouts.[2] They also estimated the neutron and capture gamma ray doses in a room made of high-density concrete and reported the effect of concrete composition on the neutron dose. Ghiasi and Mesbahi[3] utilized the MCNPX code to derive an analytical formula to calculate capture gamma ray dose equivalent in the double-bend mazes during megavoltage radiotherapy. In another publication, they characterized (n,γ) and (γ,n) photonuclear reactions in a radiation therapy bunker and derived neutron, photon, and gamma ray spectra and dose equivalents at different locations in a radiation therapy room.[20] Beigi et al. designed a safe bunker for an 18-MV linac and calculated the required thickness for barrier and door material.[14] Ghiasi and Mesbahi simulated a simplified linac model, in accordance with Swanson's reported data and compared proposed and full MC models.[15] Moreover, they simulated a medical linac in a treatment room and assessed the effect of gantry rotation on the maze entrance dose.[16]

Different applications of MCNP code for estimation of photon and neutron dose and energy spectra have been reported in the literature.[17–20] For instance, Ghasemi studied photon and photoneutron dose equivalent from a 15 MV Siemens PRIMUS and calculated thermal neutrons.[21] Chibani et al. conducted photonuclear dose calculations for 18 MV photon beams of Siemens and Varian linacs. They reported that neutron dose equivalent decreases with reduction in field size while the proton (or alpha) dose equivalent does not vary significantly, except for the 1 cm × 1 cm field. Both Varian beams (15 and 18 MV) produce more neutrons, protons, and alpha particles than the Siemens 18 MV beam. This is mainly because of their higher primary electron energies: 15 and 18.3 MeV, respectively, vs. 14 MeV for the Siemens 18 MV beam.[22] In addition to MCNP, other MC codes have been used in brachytherapy and external radiotherapy. Radiation contamination around the linac and inside the room was measured in multiple studies.[1–4,7,15–30]

Estimation of the radiation contamination components characteristics with an acceptable statistic error by MC simulation at points out of room needs high run-time. PSD file designing capability in the MC simulation method allows the user to solve the problems with complex geometry and physics, long distance from initial source to the point of estimation and in mixed radiation composed of different types of radiation transport thorough different materials in short run-time preserving precision. In full MC simulation without modelling, high run-time is needed and the method of MC may not be applicable in the above mentioned conditions. In this paper, neutron, gamma ray, linac leakage and electron contaminant radiation in distant points (points in room, maze and out of room) were estimated using the PSD file in short run-time and preserving precision. It may be considered as one of the advantages of the present work over the one component of radiation contamination estimation in low distance. Application of PSD file designing and using it for shortening the run-time and preserving the estimation precision was one of this work advantages as well as the components of radiation contamination characterization in one MC input-file running.

## 2. Aim

Our aim was to model a linac and evaluate the production of useful beam and contaminant radiation around the modeled linac. We used a phase-space distribution (PSD) file approach to enable rapid calculations and preserve the precision of the calculations. Simulation was conducted using a verified and benchmarked model for photon and other radiation characterization, inside and outside of the room. Dosimetric properties, in-field and out-of-field radiation dose, fluence, and other dosimetric characteristics were addressed in this study. We followed the TRS-398 technical report of the International Atomic Energy Agency (IAEA), in conjunction with other recommendations and reports.[31]

## 3. Materials and methods

The main parts of an 18 MV Varian C/D 2100 linac head, as well as a massive shielding assembly, were simulated in accordance with manufacturer-provided data. The linac was modeled in a typical treatment room made of ordinary concrete to simulate actual radiation scattering from room walls. A water phantom with the dimension of $50 \times 50 \times 50\ cm^3$ was simulated at a source to surface distance (SSD) of 100 from the linac target and 150 cm from the room roof. The main simulated parts that affect the photon beam and radiation contamination characteristics were as follows: the bending magnet, a Gaussian distribution of primary accelerated electrons, a tungsten target with cupper electron stopping piece, a complex iron-flattening filter and its supporting parts, primary and secondary collimators, movable jaws in the X and Y directions, mirror and ionizing chambers as well as a massive and complex shielding around the head. The distribution of incident primary electrons striking on the target was simulated as Gaussian distribution with full width at half maximum (FWHM) equal to 0.97 mm according to the primary electron distribution. Materials of these parts were simulated in accordance with manufacturer provided documents. Bunker entrance door was simulated as a sandwich configuration, composed of 15.08 cm borated polyethylene (BPE) I center, 0.48 cm steel and 1.27 cm lead as outer layers. Boron polyethylene (PE) was simulated as 5% of PE which was sandwiched between the inside lead layer and outside steel layer of 0.48 cm or 15.08 cm BPE including 5% boron in weight between the outer layers of 1.27 cm lead + 0.48 cm steel. Importantly, the inner layer of BPE in 5% Boron (w%) contained two steel and lead layers. In summary, in the construction of the bunker entrance door, a central polyethylene (5% borated) with thickness of 15 cm was sandwiched between two steel sheets with thickness of 0.48 cm on each side. Finally, these pieces were covered by two external layers of lead with thickness of 1.27 cm.

Figs. 1 and 2 show the simulated linac and room, including dose scoring points within the room and outside the room. Steel slabs inside the concrete were modeled with $7.9\ g/cm^3$ density and atomic fractions of 0.15% C, 0.30% Si, 0.50% Mg, and 99.05% Fe. Inside and outside of the modeled bunker were filled with air containing 1% moisture, at a density of $0.0012\ g/cm^3$. The composition of the air, by atomic fraction, was modeled as follows: 1.00% H, 0.02% C, 77.26% N, 21.26% O, and 0.46% Ar. The air also filled the empty space of the linac head. For reference, the source electron energy spectrum was modeled as a Gaussian distribution with a mean of 18.13 MeV and a FWHM of 1.39 MeV. The PSD surface was modeled at 1 cm lower than the flattening filter in a planar surface config-

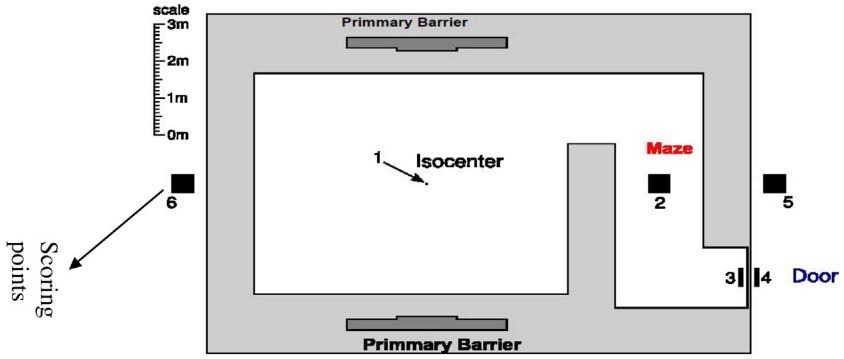


**Fig. 1.** A horizontal cross-section of the modelled bunker of an 18 MV Siemens PRIMUS linac. The light-gray areas are concrete, while the dark-grey areas are steel.

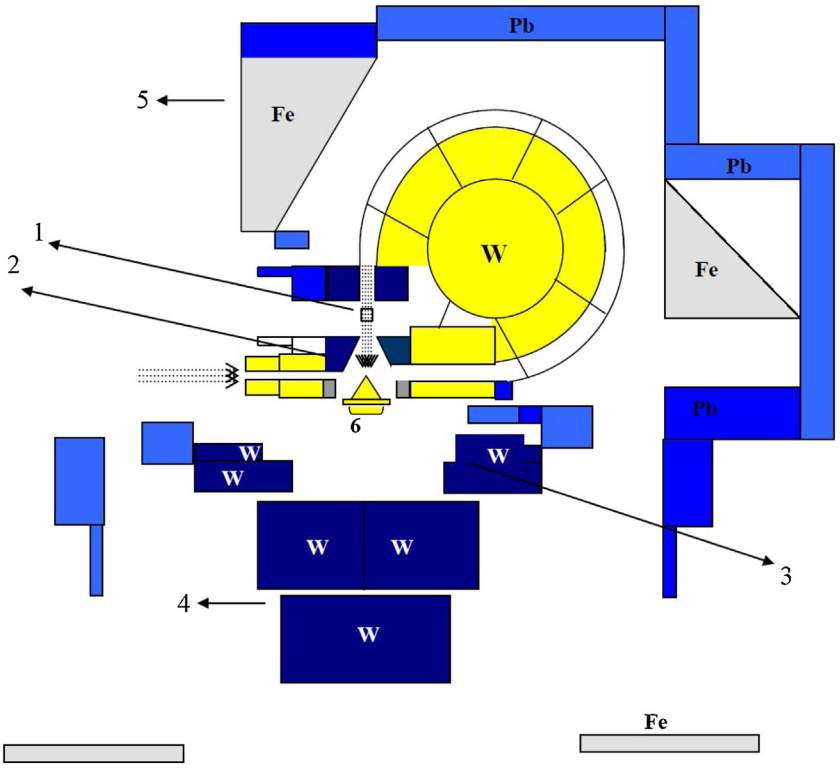


**Fig. 2.** Fully described geometry of the simulated Varian 2100 Clinac (side view). The components are: 1, primary electrons; 2, primary collimators; 3, secondary collimators; 4, moveable jaws; 5, head shielding assembly; 6, flattening filter.

uration, as the upper parts of the linac head are not movable and the lower parts, such as movable jaws, are moving during field size opening and calculations. During the initial run, all generated radiation history was registered and stored in the PSD surface. In the second run of the program, the PSD surface, including all histories, operated as the source and upper parts were removed from the MC model. Using this method, percent depth dose (PDD) and photon beam profile (PBP) were derived with only a field size opening variation of up to 15 min for each field size. During the initial run of the PSD file, $6 \times 10^7$ primary electrons and generated photons, as well as other particles, were registered in the PSD surface. With this number stored in the PSD history, the maximum statistical errors of MC results for PDD and PBP calculations were 0.004 to 0.009 within the penumbra region and at a depth of 50 cm.

Fig. 3 shows a comparison of curves obtained by MC simulation and direct measurement. One of the advantages of the PSD approach was the ability to delete most interactions of photons and elections with fixed components of the head (which remain the same for all runs) that is time-consuming. This approach reduces effectively simulation run-time from several hours to several minutes on a personal computer. Comparing the measured PDDs and PBPs, the MC model of the linac head was verified and the energy of the primary electrons was tuned and set with a real linac. The primary collimator opening angle was simulated as 14° relative to the central axis of beam.

Cylindrical cells (1 mm radius and 50 mm height) were modeled in a long cylindrical cell to score the absorbed dose and radiation fluence, at a depth of 5 cm in the phantom. Additionally, the same cells, perpendicular to the photon beam axis, simulated a beam profile calculation at 5 cm below the phantom surface.

PDDs and PBPs for field sizes of $10 \times 10$, $20 \times 20$, $30 \times 30$, and $40 \times 40$ were calculated and compared with measurements. We also derived and compared PBP in the X and Y directions and at the four edges of the simulated field sizes. Tissue-phantom-ratio ($TPR_{20,10}$) for the MC model of the linac was obtained in accordance with the Technical Report code of practice Series number

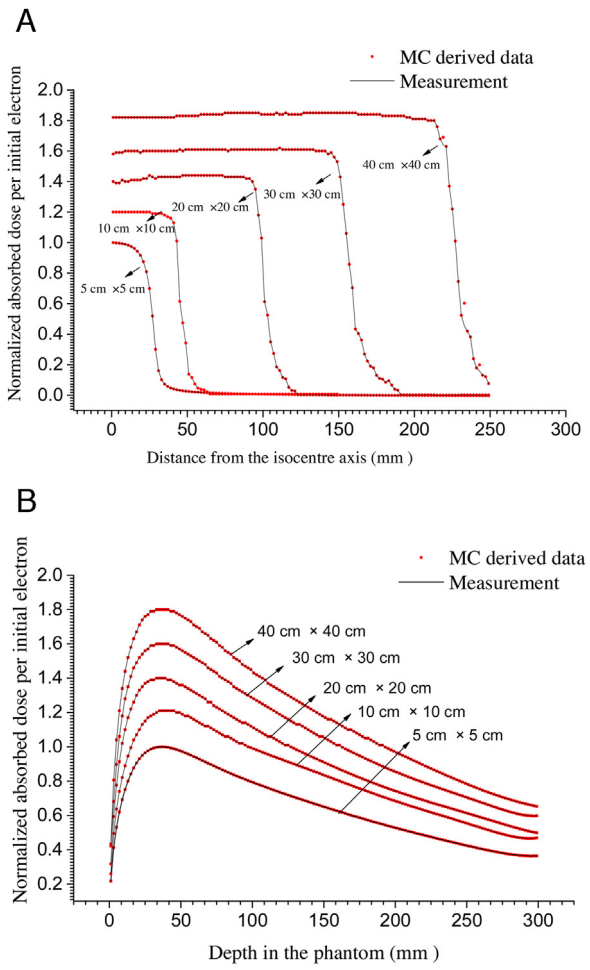


**Fig. 3.** (A) Normalized photon beam profile (PBP) in various field sizes for the linac used in the study. (B) Normalized percent depth dose (PDD) in various field sizes for the linac used in the study.

398, released by the International Atomic Energy Agency (TRS-398 code of practice of IAEA), and compared with the value derived from the real linac by measurement in a standard $10 \times 10\,cm^2$ field size, as well as other field sizes. Dosimetric data derived from measurements and the linac including PDD, PBP, $TPR_{20,10}$ for different fields were compared with the TRS-398 criteria. The dose profiles at the penumbra region were compared to the MC results and were in good agreement with measured data. The number of neutrons produced from a linac at the isocenter, normalized to the photon-absorbed dose in Gy at isocenter, was calculated. The linac model was verified to estimate photoneutron contamination and perform subsequent capture gamma ray calculations. Our resultant values and differences were reported in this paper. Furthermore, organ doses from out-of-field radiations were assessed and secondary cancer risk estimation as well as fatal/nonfatal risk estimation for the patient organs in 18 MV photon beam were performed. For dose calculations around the linac, inside and outside of the room was measured in accordance with the PSD method for other surfaces. Because of the long run-time required to obtain a result with acceptable uncertainty, a spherical surface around the linac was modeled as the PSD surface; electron/photon/neutron mode was used to run the input file and all histories around the linac were registered at the surface. For next calculations, the linac was removed from the room geometry and the PSD surface replaced the linac and operated as the source. Photon, neutron, and capture gamma ray doses were calculated at six points inside and outside of the room. After calculating the sum of photon and neutron doses, the total dose at the studied points was reported. Further, a Medical Internal Radiation Dose (MIRD) humanoid phantom was used to score a 72 Gy dose that is delivered to the prostate as the tumor and scattered radiations to other organs were estimated by the MC method. Appling the report no.103 of the International Commission on Radiological Protection (ICRP), risk estimations for the organs were performed. At 3 points, including 1 m from the isocenter on the treatment coach, inside and outside of the outer maze entrance door, thermos-luminescence (TLD) dosimetry was conducted to find TLD dose measurement. As ICRU no.26 recommendation for neutron dosimetry in mixed neutron-gamma ray mixed radiation field, TLD 600/700 pair was chosen to dosimetry; TLD 600 is sensitive to thermal neutron and TLD 700 is insensitive to thermal neutron while sensitivity to gamma was the same. TLDs employed in this study were TLD 600/700 chips with TLD reader of Harshaw 3500 reader with heating rate of 5 °C/sec in the temperature range of 30–250 °C after irradiation. TLD 600 rich of $^6Li$ wich have high thermal neutron absorpion cross-sectoion due to nuclear reaction of ($^6Li(n,\alpha)^3H$) while TLD 700 enriched for $^7Li$ (which cannot react in the above nucler reation) and cross-section of thermal neutron absorption for it is very low while sensetivity of both TLDs to gamma can be considered to be the same. Secondary Standard Dosimetry Laboratory (SSDL) irradiated and provided data to derive the calibration curve and factor. The TLDs used in this study were 3 mm × 3 mm × 0.89 mm in size and had effective atomic number ($Z_{eff}$) 8.2; therefore, the neutron dosimeters in this study can be considered as tissue-equivalent material. TLD 600 and 700 enrichment for Li isotopes was 95.6% $^6Li$ and 99.99% $^7Li$ in LiF composition of TLDs. In fact, TLD 700 poses a small amount of $^6Li$ then TLD 600 sensitivity is higher than TLD 700 while sensitivity to gamma ray is the same. According to SSDL provided data, TLD chips were first tested and those having sensivity whithin ±3% gave us to use to experimentals. Callibration curve is shown in Fig. 6. Calibration factor (CF) was 0.0034 Gy/nC according to the callibration curve wich derived the TLDs absorbed dose in Gy as a function of response in nC. Distances of 1, 14 and 20 cm were used to irradiation in the calibration process.

## 4. Results

The PSD method of MC simulation was utilized to model an 18 MV Varian 2100 Clinac. The modeled linac was rapidly verified and benchmarked for the photon and neutron calculations, using the PSD method. Our calculations revealed absorption of $1.2 \times 10^{-14}$ Gy dose from X-rays, per an initial incident electron. $8.33 \times 10^{13}$ initial electrons are needed to deliver an X-ray dose of 1 Gy ray at the isocenter. $2.50 \times 10^{14}$ initial electrons are required to simulate a 3 Gy/min photon dose-rate produced by the linac. Thus, $4.17 \times 10^{12}$/s initial electron rate is required to reach a 3 Gy/min dose rate at the isocenter. At different field sizes, the absorbed dose in the water phantom in the cylindrical cells at height and radius of 0.1 mm and 5 mm located on the central axis from the phantom surface to 20 cm below the phantom surface was scored. Datasets derived from the MC simulation method and direct measurement were compared. Tuning the primary electron energy was performed in comparison with the measured PDD data. Different PDDs were calculated from primary electron energies of 17.5–18.5 MeV. The MC calculated PDDs were compared with measured PDD. Based on the best agreement (less than 1% difference) between measured and calculated PDD, the energy of the modeled primary electron was set as 18.3 MeV. Source to isocenter distance (SID) was set as 103.3 cm. In the modeled water phantom with sides equal to 50 cm and SID as 103.3 cm, for PDD at a standard $10 \times 10\,cm^2$ field size, the differences in PDD curve between MC and measurement methods were 0.86%, 0.88%, and 1.12% at dose build-up, $d_{max}$, and descending regions, respectively. In other fields, the difference at $d_{max}$ was <1%;

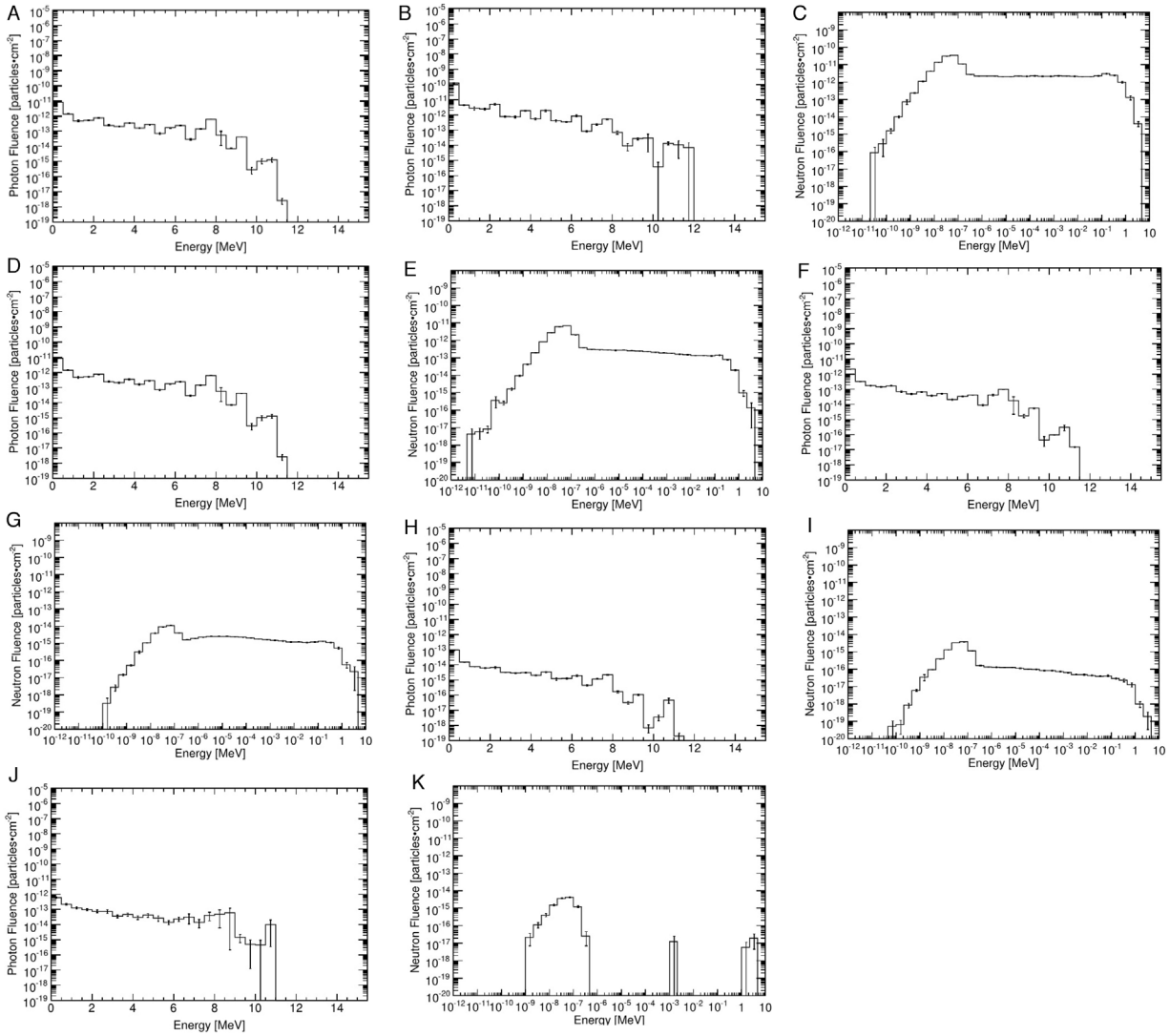


**Fig. 4.** (A) Photon spectra at location 1. (B) Photon spectra at location 2, in the maze. (C) Neutron spectra at location 2, in the maze. (D) Photon spectra at location 3, inside the door. (E) Neutron spectra at location 3, inside the door. (F) Photon spectra at location 4, outside the door. (G) Neutron spectra at location 4, outside the door. (H) Photon spectra at location 5, in the control area. (I) Neutron spectra at location 5, in the control area. (J) Photon Spectra at location 6, outside the bunker. (K) Neutron Spectra at location 6, outside the bunker.

the differences in dose build-up and descending regions were near the values obtained for the standard field size. Comparing dataset differences in these three regions of PDD curves with the TRS-398 code of practice criteria (which explain acceptable limits), the differences between the simulated model and measured data did not violate the TRS-398 criteria. The resulting data for PBP curves were compared with the measured data at the depth of 5 cm in a water phantom; the comparisons revealed that the calculated differences were below the limits of the TRS-398 code of practice criteria.

Figs. 1 and 2 show schematic views of the modeled linac, as well as PDD and photon PBP curves for studied field sizes, respectively. TPR, using the recommendations of TRS-398, was compared with the PDD parameter. $TPR_{20,10}$ is recommended to be used in calculations and has been reported as a parameter that exhibits beam penetration and energy characteristics. Thus, we calculated it according to the IAEA code of practice. MC calculated $TPR_{20,10}$ was 0.773, while direct measurements showed it as 0.774.

We calculated relevant parameters of MC model for photoneutron calculations. The most important parameter was the model's apparent neutron source strength ($Q_N$). It was defined as the number of neutrons produced by the linac when the linac delivered 1 Gy X-ray at the isocenter. $Q_N$ is in neutron per dose of isocenter n°/Gy and our MC calculations showed $Q_N$ of $1.23 \times 10^{12}$ n°/Gy X-ray at the isocenter. In this work, we calculated the primary electrons required to define the dose rate using this value. Our calculated fluence (photon/cm$^2$) at isocenter was $1.86 \times 10^{-04}$ per initial electron (photon/cm$^2$/e$_0$). According to our calculations, photon intensity at the isocenter was $7.75 \times 10^8$ (photon/cm$^2$/s). Photoneutron intensity and fluence at the isocenter were calculated as $2.65 \times 10^4$ (photon/cm$^2$/Gy X-ray) and 6.31 (n$_0$/cm$^2$/s). We calculated the photon or neutron fluence in 1 cm2 per second. Photoneutron and photon doses, equivalent at the positions marked in Fig. 1, were obtained as follows: at isocenter, photon dose was $2.4 \times 10^{-14}$ Gy per initial primary electron and neutron fluence at isocenter was 2.22 × 10-8 neutron per cm$^2$ (n$_0$/cm$^2$). Using these data, $Q_N$ was calculated as $1.34 \times 10^{12}$ n0/Gy at isocenter photon dose. Average energy of the neutrons at isocenter was scored as 0.42 MeV. Multiplication of this value in scored cells per neutron per initial electron yields neutron per Gy of photon dose at isocenter at a specific position. As seen at the location 1 (Fig. 1) in MC derived spectra for photons and neutrons, peaks of neutrons appeared at 0.7 MeV and 1.2 MeV, while for photons only a peak at 0.583 MeV was observed.

**Table 1**
Monte Carlo estimated dose equivalent in mSv/Gy.

| Location in geometry | Photon | Neutron | Total |
|---|---|---|---|
| 1 | $(1.00 \pm 0.00)) \times 10^{\circ}$ | $(1.37 \pm 0.03) \times 10^{-2}$ | $(1.01 \pm 0.03) \times 10^{\circ}$ |
| 2 | $(6.10 \pm 0.23) \times 10^{-6}$ | $(5.55 \pm 0.09) \times 10^{-5}$ | $(6.16 \pm 0.10) \times 10^{-5}$ |
| 3 | $(1.328 \pm 0.028) \times 10^{-6}$ | $(5.74 \pm 0.05) \times 10^{-6}$ | $(7.06 \pm 0.06) \times 10^{-6}$ |
| 4 | $(3.37 \pm 0.10) \times 10^{-7}$ | $(2.61 \pm 0.10) \times 10^{-8}$ | $(3.63 \pm 0.10) \times 10^{-7}$ |
| 5 | $(1.285 \pm 0.029) \times 10^{-8}$ | $(2.78 \pm 0.05) \times 10^{-9}$ | $(1.56 \pm 0.03) \times 10^{-8}$ |
| 6 | $(2.30 \pm 0.6) \times 10^{-7}$ | $(2.61 \pm 0.16) \times 10^{-9}$ | $(2.3 \pm 0.6) \times 10^{-7}$ |

**Table 2**
Photoneutron, capture gamma ray and linac leakage photon dose equivalent at out of close door (outer Maze entrance, 1 m above than floor) in mSv/Gy X at different distances.

| Distance from door | 30 cm | 50 cm | 70 cm | 90 cm | 100 cm |
|---|---|---|---|---|---|
| Photoneutron | $3.37 \times 10^{-7}$ | $1.11 \times 10^{-7}$ | $7.87 \times 10^{-8}$ | $4.84 \times 10^{-8}$ | $9.92 \times 10^{-9}$ |
| Capture gamma ray and photon from the linac | $2.61 \times 10^{-8}$ | $1.247 \times 10^{-8}$ | $1.09 \times 10^{-8}$ | $9.95 \times 10^{-9}$ | $9.83 \times 10^{-9}$ |

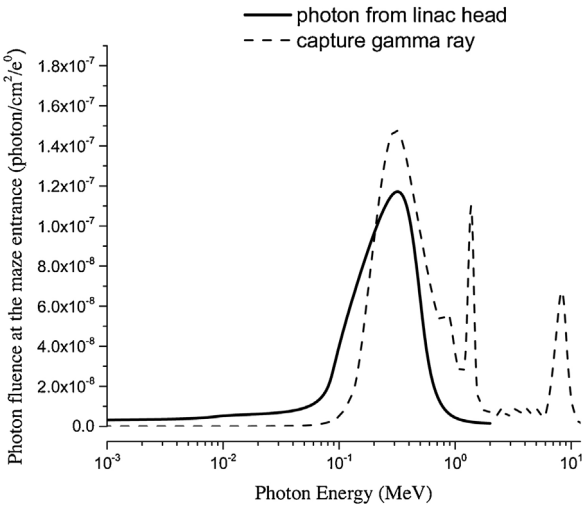


**Fig. 5.** Photons from a linac head and neutron capture gamma spectra outside door, as in location 4. Linac photons are dominant.

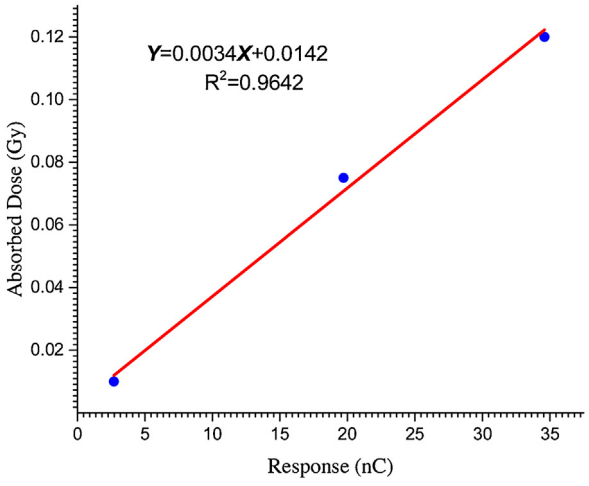


**Fig. 6.** Calibration curve for TLD 600/700. Ra-Be source employed to irradiation of the TLD 600/700 pairs at 7, 14 and 20 cm to calibration of the dosimeters to neutron dosimetry in this study.

Dose equivalent and ambient dose equivalent were calculated for all six marked points and tabulated in Table 1. The effect of the door on dose attenuation for photon, neutron, and total dose is also tabulated in Table 2. In Fig. 1, Points 5 and 6 are located outside of the room and the effect of the walls in radiation reduction was found by dose scoring inside and outside of the room. In addition to dose calculation at different points in the bunker, spectra analysis was conducted at the same locations. Further, using a humanoid phantom, simulation of prostate radiotherapy with 36 fractions and 2 Gy per fraction was performed. The secondary cancer risk was calculated for different organs. Notably, photon dose equivalent was reduced by approximately $4.34 \times 10^6$ times at location 6 outside the bunker relative to isocenter. Additionally, the door attenuated photon and neutron doses by 4 and 10 times, respectively, as shown in Table 1. A considerable reduction was observed in both neutron and photon dose within the maze at location 5 outside the maze. Photon dose equivalents at 50 cm above and around the target of the modeled linac were estimated as 0.0051 and 0.0028 mSv/Gy of X-ray at isocenter. The results of TL dosimetry for the photoneutron at the distance of 1 m from the isocenter on the treatment coach, inner and outer maze door points showed a small difference with MC results. Difference at point 1 or isocenter were 2.47%, 2.77% and 2.89%, respectively, for photoneutron dose. Additionally, photon and neutron spectra analyses were conducted, using the F4 tally of the MC code at the locations shown in the room geometry. Derived spectra are shown in a logarithmic scale in Fig. 4. At the maze entrance, capture gamma ray spectra, due to photoneutron contamination as well as linac leakage photons were derived using the F4 tally of MC with narrow energy bins. The spectra were shown in Fig. 5. According to our estimations and derived energy fluence at isocentre and maze entrance it was seen that only 11% of the neutrons at isocenter were fast and epithermal and 89% of the neutrons were thermal. Thermal neutrons have a negligible portion in delivered dose equivalent at patient body and isocenter. But, in the maze and maze entrance, thermal neutrons are dominant and dose from the neutron is dose from the thermal/resonance neutrons.at the maze entrance, peak of neutron energy fluence observed at energy range and number of neutrons as follows. MC simulations scored neutrons energy fluence in narrow bins from $3.66 \times 10^{-7}$ to 3 MeV at the maze entrance and it was found that energy range of $2.90 \times 10^{-6}$–$3.66 \times 10^{-5}$ MeV had higher number of neutrons at the maze entrance with $2.03 \times 10^{-8}$–$1.29 \times 10^{-8}$ neutrons. For photons from the linac head at maze entrance, in energies of 0.04, 0.10 and 0.85 MeV the number of photons as $7.58 \times 10^{-9}$, $4.28 \times 10^{-8}$ and $6.75 \times 10^{-9}$ are the peak of photons in the spectrum. For capture gamma ray energies also 0.151, 0.518, 1.64, 4.25, 5.25, 8.45 MeV having $2.48 \times 10^{-8}$, $9.12 \times 10^{-8}$, $1.54 \times 10^{-8}$, $1.12 \times 10^{-8}$, $1.02 \times 10^{-8}$, $7.85 \times 10^{-8}$ gamma ray photons due to neutron capture made peaks in the energy fluence.

## 5. Discussion

In the current study, photoneutron and subsequently generated capture gamma ray dose and fluence were investigated. Our method comprised of the computational PSD approach of the MC method. The PSD approach reduced run-time while decreasing

computational statistical error. Our linac model was verified and benchmarked using a measurement dataset for PDD and PBP comparisons. Further, the model of linac was verified for the neutron calculations by deriving the linac $Q_N$. We obtained a value that is slightly higher than the previously reported value for the same model and operating machine. The difference may be attributed to the presence of room walls. Reported values were calculated around an in-air linac model, whereas our result was calculated for a linac in a bunker. In our previous publication, it was revealed that room walls can be a photoneutron source, which other publications have also reported.[13,25–28] Additionally, the steel slab in the concrete may cause increased neutron production because of the high atomic number of the steel. According to the maze dimensions, room height, room inner surface and other characteristics of the room and of the machine, such as $Q_N$ and delivering X-ray photon dose to isocenter, dose level at door location can be different. Our simulated door reduced dose level to acceptable dose level (0.1 mSv per week, 5 days and 8 h working time per day) in the geometry and linac as well as material of the room walls. Konefal et al. and delivering X-ray photon dose to isocenter, dose level at door location can be different. Our simulated door reduced dose level to acceptable dose level (0.1 mSv per week, 5 days and 8 h working time per day) in the geometry and linac as well as material of the room walls. Konefal et al.[22–34] In their study, they proposed a significant change in the design of a door to a room with slowed down neutron field by means of commonly used inexpensive protective materials and proposed a door composition and material.[24] Our simulated door is similar to that designed by Konefal et al.[24] in material and different from their door in dimensions. Our designed door reduced the dose to below the acceptable level in our geometry and linac characterizations such as $Q_N$ value of linac, walls materials and room and maze dimensions. Differences in BPE, steel and lead thickness in relation to the work of Konefal et al.[24] may be attributed to the difference in machine and room characteristics. Photon and neutron spectra, inside and outside of the bunker, were in agreement with other studies.[30–40] Different investigations regarding the neutron and photon dose in the bunker support our results. Dose estimation and shielding evaluations for out of room points have not been conducted extensively and radiation characterization in control room and out of treatment room were needed. Although it is time-consuming and difficult to reach an acceptable level of statistical error, we used the PSD method and showed that time-consuming runs could finish in <28 min, with statistical errors of $\leq$0.012. Using the PSD method, we calculated the dose and spectra around the linac, as well as inside and outside of the bunker. Several studies regarding the photoneutron dose and spectra analysis during megavoltage radiotherapy support our results. For instance, our MC derived spectra were in close agreement with the results of Israngul-NA et al.[52] in terms of prompt gamma ray analysis and also in each spectrum, an annihilation peak can be seen.[41] The authors proposed additional work on this issue to improve the investigations. Regarding the room effect on the radiation attenuation, as well as door composition, some researchers have evaluated the neutron and gamma ray attenuation factor and their results support our observations.[41–51]

## 6. Conclusions

In the current study, photoneutron, prompt capture gamma ray, electron contamination and linac leakage photons were characterized. It was seen that prompt gamma ray photons are dominant at maze entrance and electron contamination was found only in-field and slightly around the useful beam. Furthermore, photoneutron propagated from target to outside of the room. Each component was characterized using PSD file designing. Additionally, it was revealed that application of the PSD approach in this study efficiently reduced run-time while preserving the estimation precision. Our findings showed that PSD approach was more effective than full MC simulation in solving the radiation transport problems, especially in complex geometry and physics of the problem and long distances of radiation source to the estimation point. The authors recommend PSD file employment in radiation dosimetry for complex geometry and when radiation transport in a long distance is needed.

## Conflict of interest

None declared.

## Financial disclosure

None declared.

## References

1. Ghiasi H, Mesbahi A. Monte Carlo characterization of photoneutrons in the radiation therapy with high energy photons: a comparison between simplified and full Monte Carlo models. *IJRR*. 2010;1(8):187–193.
2. Mesbahi Asghar, Ghiasi Hosein, Mahdavi Seyed Rabee. Photoneutron and capture gamma dose equivalent for different room and maze layouts in radiation therapy. *Rad Protect Dosim*. 2010;140:242–249.
3. Ghiasi H, Mesbahi A. A new analytical formula for neutron capture gamma dose calculations in double-bend mazes in radiation therapy. *Rep Pract Oncol Radiother*. 2012;17:220–225.
4. Beigi M, Afarande F, Ghiasi H. Safe bunker designing for the 18MV Varian 2100 Clinac: a comparison between Monte Carlo simulation based upon data and new protocol recommendations. *Rep Pract Oncol Radiother*. 2016;21:42–49.
5. Ghiasi Hosein, Mesbahi Asghar. Monte Carlo characterization of photoneutrons in the radiation therapy with high energy photons: a comparison between simplified and full Monte Carlo models. *Int J of Radiat Reas*. 2010;8:187–193.
6. Ghiasi Hosein, Mesbahi Asghar. Gantry orientation effect on the neutron and capture gamma ray dose equivalent at the maze entrance door in radiation-therapy. *Nucl Tech and Radiat Protect*. 2012;17:220–225.
7. Schneider U, Hälg RA, Lomax T. Neutrons in active proton therapy: Parameterization of dose and dose equivalent. *Zeitschrift für Medizinische Physik*. 2017;27(2):113–123.
8. ICRU. *International Commission on Radiation Units and measurement. Neutron Dosimetry for Biology and Medicine*; 1977. Report 26.
9. Sohrabi M, Hakimi A. Fast, epithermal and thermal photoneutron dosimetry in air and in tissue equivalent phantom for a high-energy X-ray medical accelerator. *Zeitschrift für Medizinische Physik*. 2017;23, in press.
10. Faby S, Wilkens JJ. Assessment of secondary radiation and radiation protection in laser-driven proton therapy. *Zeitschrift für Medizinische Physik*. 2015;25(2):112–122.
11. Ghiasi H, Mesbahi A. Monte carlo characterization of photoneutrons in the radiation therapy with high energy photons: a comparison between simplified and full Monte Carlo models. *Int J of Radiat Research*. 2010;8(3):187–193.
12. Brkiç H, Ivkovç A, Kasabaiç M, et al. The influence of field size and off-axis distance on photoneutron spectra of the 18MV siemens oncor linear accelerator beam. *Radiat Meas*. 2016;93:28–34.
13. Ghiasi H, Mesbahi A. Sensitization of the analytical methods for photoneutron calculations to the wall concrete composition in radiation therapy. *Radiat Meas*. 2012;47:461–464.
14. Juste B, Morato S, Miro R, Verdu G, Diez S. MCNP6 unstructured mesh application to estimate the photoneutron distribution and induced activity inside a linac bunker. *Radiat Phys Chem*. 2017;137:18–22.
15. Mesbahi A, Dadgar H, Ghareh-Aghaji N, Mohammadzadeh M. A Monte Carlo approach to lung dose calculation in small fields used in intensity modulated radiation therapy and stereotactic body radiation therapy. *J Cancer Res Ther*. 2014;10:896–902.
16. Mesbahi A, Haghzadeh A, Naseri AR, Shirazi AR. Monte carlo calculation of shielded colpostat effect on rectum received dose in high dose rate brachytherapy with cobalt-60 sources. *Int J of Radiat Rea*. 2015;13(2):165–171.
17. Mesbahi A, Azarpeyvand AA, Shirazi A. Photoneutron production and backscattering in high density concretes used for radiation therapy shielding. *Ann Nucl Energy*. 2011;38:2752–2756.
18. Mohammadi A, Afarideh H, Abbasi Davani F, Arbabi A. New aspect determination of photoneutron contamination in 18_ÈMV medical linear accelerator. *Radiat Meas*. 2016;95:55–61.
19. Shweikani R, Anjak O. Estimation of photoneutron intensities around radiotherapy linear accelerator 23-MV photon beam. *Appl Radiat Isot*. 2015;99:168–171.
20. Ghiasi H. Monte Carlo characterizations mapping of the (γ,n) and (n,γ) photonuclear reactions in the high energy X-ray radiation therapy. *Rep Pract Oncol Radiother*. 2014;19(1):30–36.

21. Ghasemi A, Pourfallah TA, Akbari MR, Babapour H, Shahidi M. Photo neutron dose equivalent rate in 15 MV X-ray beam from a Siemens Primus Linac. *J Med Phys*. 2015;40(2):90–94.
22. Kelleter L, Wrońska A, Besuglow J, et al. Spectroscopic study of prompt-gamma emission for range verification in proton therapy. *Phys Med*. 2017;34:7–17.
23. Khajetash B, Bahreyni Toossi MT, Ghorbani M, Jahangiri M, Akbari F. Measurement of fast neutron contamination caused by the presence of wedge and block using CR-39 detector. *J Cancer Res Ther*. 2019;15:S103–S109.
24. Konefał A, Łaciak M, Dawidowska A, Osewski W. Significant change in the construction of a door to a room with slowed down neutron field by means of commonly used inexpensive protective materials. *Radiat Prot Dosimetry*. 2014;162(3):197–207.
25. Konefał A, Orlef A, Laciak M, Ciba A, Szewczuk M. Thermal and resonance neutrons generated by various electron and X-ray therapeutic beams from medical linacs installed in polish oncological centers. *Rep Pract Oncol Radiother*. 2012;17(6):339–346.
26. Polaczek-Grelik K, Karaczyn B, Konefał A. Nuclear reactions in linear medical accelerators and their exposure consequences. *Appl Radiat Isot*. 2012;70(10):2332–2339.
27. Konefał A, Orlef A, Dybek M, Maniakowski Z, Polaczek-Grelik K, Zipper W. Correlation between radioactivity induced inside the treatment room and the undesirable thermal/resonance neutron radiation produced by linac. *Phys Med*. 2008;24(4):212–218.
28. Konefal A, Polaczek-Grelik K, Zipper W. Undesirable nuclear reactions and induced radioactivity as a result of the use of the high-energy therapeutic beams generated by medical linacs. *Radiat Prot Dosimetry*. 2008;128(2):133–145.
29. Pietrzak P, Konefał A, Sokół M, Orlef A. Comparison of depth-dose distributions of proton therapeutic beams calculated by means of logical detectors and ionization chamber modeled in Monte Carlo codes. *Nucl Instrum Methods Phys Res Sect A*. 2016;826:55–59.
30. Konefał A, Bakoniak M, Orlef A, Maniakowsk Z, Szewczuk M. Energy spectra in water for the 6 MV X-ray therapeutic beam generated by Clinac-2300 linac. *Radiat Meas*. 2015;72:12–22.
31. Dawidowska A, Paluch MF, Konefał A. The determination of a dose deposited in reference medium due to (p,n) reaction occurring during proton therapy. *Rep Pract Oncol Radiother*. 2014;19:s3–s8.
32. Konefał A, Orlef A, Bieniasiewic M. Measurements of neutron radiation and induced radioactivity for the new medical linear accelerator, the Varian TrueBeam. *Radiat Meas*. 2016;86:8–15.
33. Bieniasiewicz M, Konefał A, Wendykier J, Orlef A. Measurements of thermal and resonance neutron fluence and induced radioactivity inside bunkers of medical linear accelerators in the center of oncology in Opole. *Poland. Acta Physica Polonica Series B*. 2016;47(3):771–776.
34. Konefał A, Dybek M, Zipper W, Łobodziec W, Szczucka K. Thermal and epithermal neutrons in the vicinity of the Primus Siemens biomedical accelerator. *Nukleonika*. 2005;50(2):73–81.
35. Azorín C, Vega-Carrillo HR, Rivera T, Azorín J. Calculation of fluence and absorbed dose in head tissues due to different photon energies. *Appl Radiat Isot*. 2014;83:230–234.
36. Vega-Carrillo HR, Ortiz-Rodríguez JM, Martínez-Blanco MR. NSDUAZ unfolding package for neutron spectrometry and dosimetry with Bonner spheres. *Appl Radiat Isot*. 2012;71:87–91.
37. Benavente JA, Vega-Carrillo HR, Lacerda MAS, Fonseca TCF, da Silva TA. Neutron spectra due 13N production in a PET cyclotron. *Appl Radiat Isot*. 2015;99:20–24.
38. Ortiz-Rodríguez JM, Alfaro R, Haro R, Cervantes Viramontes JM, Vega-Carrillo HR. A neutron spectrum unfolding computer code based on artificial neural networks. *Radiat Phys Chem*. 2014;95:428–431.
39. Vega-Carrillo HR, Hernández-Dávila VM, Aguilar F, Paredes L, Rivera T. Neutron spectra at two beam ports of a TRIGA Mark III reactor loaded with HEU fuel. *Appl Radiat Isot*. 2014;83:252–255.
40. Vega-Carrillo HR, Navarro Becerra JA, Pérez Arrieta ML, Pérez-Landeros LH. Doses in sensitive organs during prostate treatment with a 60Co unit. *Appl Radiat Isot*. 2014;83:227–229.
41. Vega-Carrillo HR, Martínez-Ovalle SA, Lallena AM, Mercado GA, Benites-Rengifo JL. Neutron and photon spectra in LINACs. *Appl Radiat Isot*. 2012;71:75–80.
42. Furetta C, Roman J, Rivera T, Azorín J, Vega-Carrillo HR. Modeling the thermoluminescent response of CaSO4:Dy by the MCNPX method. *Appl Radiat Isot*. 2010;68(4-5):967–969.
43. Vega-Carrillo HR, Villagrana-Muñoz LE, Rivera-Perez E, de Leon-Martinez HA, Hernández-Davila VM. Concrete enclosure for shielding a neutron source. *Appl Radiat Isot*. 2013;79:37–41.
44. El-Khayatt AM. NXcom – A program for calculating attenuation coefficients of fast neutrons and gamma-rays. *Ann Nucl Energy*. 2011;38(1):128–132.
45. El-Khayatt AM, Akkurt I. Photon interaction, energy absorption and neutron removal cross section of concrete including marble. *Ann Nucl Energy*. 2013;60:8–14.
46. Yılmaz E, Baltas H, Kırıs E, Ustabas I, El-Khayatt AM. Gamma ray and neutron shielding properties of some concrete materials. *Ann Nucl Energy*. 2011;38(10):2204–2212.
47. Akkurt I, El-Khayatt AM. The effect of barite proportion on neutron and gamma-ray shielding. *Ann Nucl Energy*. 2013;51:5–9.
48. İçelli O, Singh Mann K, Yalçın Z, Orak S, Karakaya V. Investigation of shielding properties of some boron compounds. *Ann Nucl Energy*. 2013;55:341–350.
49. Kurudirek M, El-Khayatt AM, Gerward L. Remarks on the extension and validity of an empirical formula for the fast-neutron removal cross-section: the effective atomic weight. *Ann Nucl Energy*. 2014;70:230–232.
50. El-Khayatt AM, Ali AM, Singh VP. Photon attenuation coefficients of Heavy-Metal Oxide glasses by MCNP code, XCOM program and experimental data: a comparison study. *Nucl Instrum Methods Phys Res A*. 2014;735:207–212.
51. El-Khayatt AM. Semi-empirical determination of gamma-ray kerma coefficients for materials of shielding and dosimetry from mass attenuation coefficients. *Prog Nucl Energy*. 2017;98:277–284.
52. Israngkul-Na-Ayuthaya Isra, Suriyapee Sivalee, Pengvanich Phongpheath. Evaluation of equivalent dose from neutrons and activation products from a 15-MV X-ray LINAC. *J Radiat Res*. 2015;56(6):919–926.